Acta Med. Okayama, 2022
Vol. 76, No. 1, pp. 25–32

Acta Medica Okayama
http://escholarship.lib.okayama-u.ac.jp/amo/

Original Article

Development and Evaluation of a Short-time Imaging Method for the Clinical Study of the Apparent Diffusion Coefficient Subtraction Method

Kohei Sugimoto[a,b], Masahiro Kuroda[a*], Yuuki Yoshimura[a,c], Kentaro Hamada[a], Abdullah Khasawneh[d], Majd Barham[d], Nouha Tekiki[d], Kohei Konishi[a,e], Hinata Ishizaka[a], Yudai Shimizu[d], Yuki Nakamitsu[a], Wlla E. Al-Hammad[d], Ryo Kamizaki[a], Susumu Kanazawa[f], and Junichi Asaumi[d]

[a]*Radiological Technology, Graduate School of Health Sciences, Okayama University, Departments of* [d]*Oral and Maxillofacial Radiology,* [f]*Radiology, Okayama University Graduate School of Medicine, Dentistry and Pharmaceutical Sciences, Okayama 700-8558, Japan,*
[b]*Divisions of Imaging Technology, Okayama Diagnostic Imaging Center, Okayama 700-0913, Japan,*
[c]*Radiology Diagnosis, Okayama Saiseikai General Hospital, Okayama 700-8511, Japan,*
[e]*Departments of Radiology, Red Cross Okayama Hospital, Okayama 700-8607, Japan*

The apparent diffusion coefficient subtraction method (ASM) was developed as a new restricted diffusion-weighted imaging technique for magnetic resonance imaging (MRI). The usefulness of the ASM has been established by *in vitro* basic research using a bio-phantom, and clinical research on the application of the ASM for the human body is needed. Herein, we developed a short-time sequence for ASM imaging of the heads of healthy volunteers (n = 2), and we investigated the similarity between the obtained ASM images and diffusion kurtosis (DK) images to determine the utility of the ASM for clinical uses. This study appears to be the first to report ASM images of the human head. We observed that the short-time sequence for the ASM imaging of the head can be scanned in approx. 3 min at 1.5T MRI. The noise reduction effect of median filter processing was confirmed on the ASM images scanned by this sequence. The obtained ASM images showed a weak correlation with the DK images, indicating that the ASM images are restricted diffusion-weighted images. The new short-time imaging sequence could thus be used in clinical studies applying the ASM.

Key words: apparent diffusion coefficient, apparent diffusion coefficient subtraction method, diffusion kurtosis imaging, restricted diffusion, short-time imaging

Diffusion kurtosis (DK) imaging is a technique for imaging restricted diffusion *in vivo* when using magnetic resonance imaging (MRI), in which the kurtosis is the degree of deviation from free diffusion in diffusion-weighted (DW) images [1, 2]. Clinical studies of DK imaging have reported its high sensitivity for acute cerebral infarction and multiple sclerosis and its usefulness for grading brain tumors [3-7]. Our group developed the apparent diffusion coefficient (ADC) subtraction method (ASM), which is an imaging method to depict restricted diffusion based on a different principle from that of DK imaging [8]. The ASM is expected to be clinically useful because it may depict restricted diffusion in the extracellular space, similar to DK imaging [8].

The existing studies of ASM used only phantoms for *in vitro* evaluations, and they did not verify whether ASM images of the human body depict the same restricted diffusion as DK images [8-10]. For the vali-

Received April 3, 2021; accepted August 3, 2021.
*Corresponding author. Phone: +81-86-235-6873; Fax: +81-86-235-6873
E-mail: kurodamd@cc.okayama-u.ac.jp (M. Kuroda)

Conflict of Interest Disclosures: No potential conflict of interest relevant to this article was reported.

dation of the usefulness of ASM images, it is necessary to develop an ASM imaging sequence that can be used in clinical practice. In addition, clinical imaging requires shorter imaging times, and the reported acquisition times for phantoms are too long for *in vivo* imaging.

As a preliminary step for future clinical research, in the present study we developed a short-time ASM imaging sequence for the human head that can be used with 1.5 and 3.0T MRI. To the best of our knowledge, this study is the first to report ASM imaging of human subjects. We also investigated the possibility of reducing the imaging time for human subjects by examining the ASM images produced by the developed imaging sequence, and we assessed the possibility of imaging restricted diffusion in the human head by comparing ASM images with DK images.

Subjects and Methods

Subjects. The imaged subjects were two healthy adult volunteers (a 26-year-old male and a 36-year-old male) who provided written informed consent and agreed to the use of their data in scientific research. The study was approved by the Ethics Committee of Okayama University (approval no. RIN 1910-004).

DW imaging and the reduction of the imaging time. A 1.5T MRI system (Magnetom Avanto fit VE11C; Siemens, Munich, Germany) and a 3.0T MRI system (Magnetom Skyra VE11C; Siemens) were used. The Head/Neck 20 was used as the receiver coil. The head of one subject was imaged using 1.5T, and the other subject's head was imaged using 3.0T MRI. The imaging conditions used for the DW imaging are shown in Table 1. Readout segmentation of long variable echo-trains [11] was used for the DW imaging. Table 2 shows the three protocols and the imaging time for each protocol.

Protocol 1 had the highest number of b-values (5 points) and the DW imaging time for ASM imaging was as long as 7 min 32 sec on 1.5T MRI. Protocol 3 had the lowest number of b-values (2 points) and the imaging time was as short as 3 min 10 sec on 1.5T MRI. Protocol 2 was an intermediate between protocols 1 and 3. The imaging time of the 3.0T MRI is slightly longer than that of the 1.5T MRI. ASM images were

Table 1 Conditions of diffusion weighted imaging

Parameters	DWI-1.5T		DWI-3.0T	
	Basic	Modify	Basic	Modify
Sequence	RESOLVE	RESOLVE	RESOLVE	RESOLVE
TR (msec)	4,860	4,860	6,450	6,450
TE (msec)	76	127	70	123
ES (msec)	0.44	0.44	0.36	0.36
FOV (mm)	220	220	220	220
Matrix	140 × 140	140 × 140	140 × 140	140 × 140
BW (Hz/pixel)	1,116	1,116	940	940
b-value (sec/mm^2)	0, 250, 500, 750, 1,000, 2,000	0, 250, 500, 750, 1,000, 10,000	0, 250, 500, 750, 1,000, 2,000	0, 250, 500, 750, 1,000, 10,000
Averages	1 (b = 0–1000), 2 (b = 2000)	1	1 (b = 0–1000), 2 (b = 2000)	1
Segments	3	3	5	5
Slice thickness (mm)	5	5	5	5
Slice number	23	23	23	23
Phase direction	AP	AP	AP	AP
δ (msec)	16.8	42.3	16.2	42.7
Δ (msec)	37.4	62.9	34.2	60.7
Diffusion time (msec)	31.8	48.8	28.8	48.8
Diffusion mode	3-Scan trace	3-Scan trace	3-Scan trace	3-Scan trace
Diffusion direction	3	3	3	3

DWI, diffusion weighted imaging; RESOLVE, readout segmentation of long variable echo-trains; TR, repetition time; TE, echo time; ES, echo space; FOV, field of view; BW, band width; AP, antero-posterior; δ, motion probing gradient (MPG) pulse duration; Δ, MPG pulse spacing. DWI-1.5T and DWI-3.0T represent DWI using 1.5 and 3.0T MRI, respectively. 'Basic' and 'modify' represent the sequences with short and long diffusion time, respectively.

Table 2 Combination of b-value and magnetic resonance imaging time for each protocol to create apparent diffusion coefficient subtraction method images

	Protocol 1		Protocol 2		Protocol 3	
	Basic	Modify	Basic	Modify	Basic	Modify
b-value (sec/mm^2)	0	0	0	0	0	0
	250	250	–	–	–	–
	500	500	500	500	–	–
	750	750	–	–	–	–
	1,000	1,000	1,000	1,000	1,000	1,000
	–	10,000	–	10,000	–	10,000
Imaging time of 1.5T (min : sec)	3 : 24	4 : 08	1 : 57	2 : 40	1 : 13	1 : 57
Imaging time of 3.0T (min : sec)	7 : 19	8 : 55	4 : 05	5 : 42	2 : 28	4 : 05

Each protocol consists of the different combinations of b-values, which decide each imaging time shown in this table. 'Basic' and 'modify' represent the sequences with short and long diffusion time, respectively.

created from DW images scanned by these three protocols, and their image quality was compared both visually and quantitatively.

Preparation of ASM images from DW images. DW images for each b-value of the 'basic' and 'modify' sequences were prepared for each protocol in Table 2. The ADC_b value was calculated for each pixel of the DW image scanned with each b-value of the 'basic' sequence according to Eq. (1):

$$ADC = \ln (S_0 - S)/b \quad (1)$$

where b is the b-value, S is the signal intensity value, and S_0 is the signal intensity value when $b = 0$ sec/mm^2. Based on Eq. (1), the ADC value is the first-order coefficient when the b-value and the logarithm of the signal intensity value are approximated by a linear function using the least-squares method. Similarly, the ADC_m value was calculated from DW images scanned with the 'modify' sequence.

Next, using each pixel value of ADC_b and ADC_m, the ASM value of each pixel was calculated according to Eq. (2) [8]:

$$ASM = |ADC_b - ADC_m|/(ADC_b)^3 \quad (2)$$

The ASM image was obtained by reconstructing the ASM values of each pixel as an image. To create this ASM image, the ASM imaging software developed by Hamada *et al.* [10] was used with certain modifications. Briefly, this software uses the image analysis software ImageJ (ver. 1.52a; National Institutes of Health, MD, USA) [12] to perform inter-image calculations according to Eq. (2) to create an ASM image. ASM images for each subject can be created in 5 min using this software.

Creation of a DK image from a DW image. A DK image was created using the following procedure for comparison as a reference-restricted DW image. DW images were prepared for each b-value of the 'basic' sequence in protocol 1. Mean kurtosis (MK) values were calculated for each pixel of the DW image scanned at each b-value of the 'basic' sequence based on Eq. (3):

$$MK = 6 \times [\ln (S - S_0) + b \times ADC]/(b^2 \times ADC^2) \quad (3)$$

where b is the b-value, S is the signal intensity value, and S_0 is the signal intensity value when $b = 0$ sec/mm^2. The first and second coefficients of the quadratic function approximating the b-value and the logarithm of the signal intensity value were used to calculate the ADC and MK values. The least-squares method was used for fitting the model to the data. The MK values of each pixel were reconstructed as an image to obtain the DK image. The images were created using Python (ver. 3.6.10; Python Software Foundation, DE, USA).

Noise reduction of images using a filter. A median filter (radius 2.0) was applied to the ASM and DK images to reduce the salt-and-pepper noise, using ImageJ (ver. 1.52a). A median filter (radius 2.0) replaces each pixel with the median value in its 3×3 neighborhood pixels of the ASM and DK images.

Statistical analysis. We used Spearman's rank correlation coefficient to examine both the similarity of ASM images created by each protocol and the similarity between ASM and DK images by using the pixel values of all pixels in the region of interest (ROI) in the images. ROIs were set in the entire brain parenchyma excluding the skull on one slice at the level of the basal ganglia for both the ASM and DK images. For the evaluation of the

effect of median filter processing, we obtained the mean, standard deviation (SD), signal to noise ratio (SNR), and coefficient of variance (CV) from the ROIs of the globus pallidus and thalamus. The SNR was calculated by dividing the mean of the pixel values by the SD in the ROIs, and the CV is the reciprocal of the SNR. The homogeneity of group variances was examined using the Fligner-Killeen test [13] by R (ver. 4.0.1; The R Foundation, Vienna, Austria). Significant differences in the variability of pixel values in the ROIs of the globus pallidus and thalamus were evaluated before and after median filter processing. *P*-values <0.05 were accepted as significant.

Results

Comparison of imaging protocols to shorten the imaging time of DW imaging for ASM imaging. The left three columns in Fig. 1 show ASM images obtained by the three different protocols with different imaging times and b-values. There is no significant visual difference between the images scanned by the three protocols at 1.5 or 3.0T.

The Spearman's rank correlation coefficient between pairs of protocols was calculated for all of the pixel values in the ROI set in the entire brain parenchyma, as shown in Table 3. The correlation coefficients between protocols 1 and 2 and between protocols 1 and 3 were both 0.84 ($p<0.01$), while the correlation coefficient between protocols 2 and 3 was 1.00 ($p<0.01$) at 1.5 and 3.0T. These results show a significantly strong correlation among all protocols. We thus selected protocol 3 (with the least number of b-values), *i.e.*, the protocol with the shortest imaging time, as the best protocol and used it in the subsequent studies.

Image quality improvement by noise reduction filter on ASM images. The fourth column from the left in Fig. 1 shows the ASM images after median filter processing. The post-filtered ASM images had visually and qualitatively less salt-and-pepper noise compared to that

Table 3 Comparison of apparent diffusion coefficient subtraction method images obtained with different imaging protocols

Imaging	Protocol 1 vs. 2	Protocol 1 vs. 3	Protocol 2 vs. 3
ASM-1.5T	0.84*	0.84*	1.00*
ASM-3.0T	0.84*	0.84*	1.00*

ASM, apparent diffusion coefficient subtraction method; *, $p<0.01$. ASM-1.5T and ASM-3.0T represent ASM using 1.5 and 3.0T MRI, respectively. The values in each cell mean Spearman's rank correlation coefficient using the signal values at the same position in ASM images scanned with different imaging protocols.

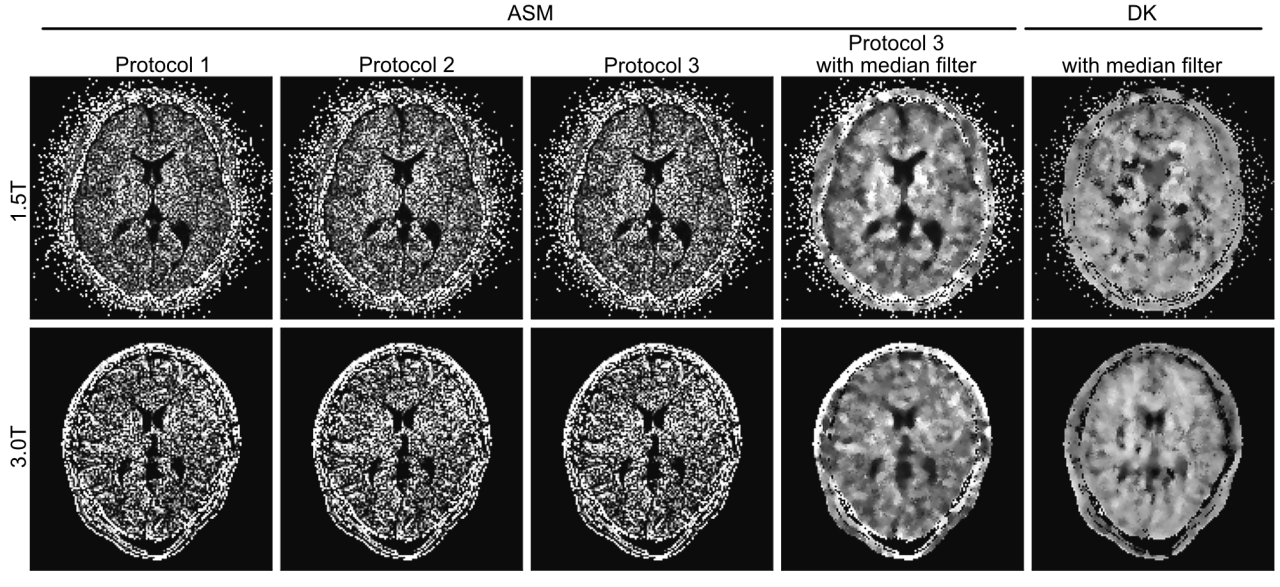

Fig. 1 ASM and DK images. From left to right, ASM images created by protocol 1, protocol 2, protocol 3, and protocol 3 with median filter processing, and DK images with median filter processing. The images in the first and second rows were scanned with 1.5 and 3.0T MRI, respectively. ASM, apparent diffusion coefficient subtraction method; DK, diffusion kurtosis.

Table 4 Region of interest values for the globus pallidus and thalamus in apparent diffusion coefficient subtraction method images before and after median filter processing

Imaging	Index	Globus pallidus		Thalamus	
		Non-filter	Median filter	Non-filter	Median filter
ASM-1.5T	N	113	113	213	213
	Mean	2.47×10^5	2.44×10^5	3.97×10^5	2.82×10^5
	SD	2.48×10^5	0.842×10^5	5.36×10^5	0.674×10^5
	SNR	1.00	2.90	0.74	4.19
	CV	1.00	0.345	1.35	0.239
	Fligner-killeen test	$p<0.01$		$p<0.01$	
ASM-3.0T	N	125	125	139	139
	Mean	4.50×10^5	3.18×10^5	3.91×10^5	3.05×10^5
	SD	3.74×10^5	0.767×10^5	3.79×10^5	0.890×10^5
	SNR	1.21	4.14	1.03	3.43
	CV	0.830	0.241	0.969	0.292
	Fligner-killeen test	$p<0.01$		$p<0.01$	

ASM, apparent diffusion coefficient subtraction method; N, number of pixels in the region of interest; SD, standard deviation; SNR, signal to noise ratio; CV, coefficient of variance. The *P*-value was calculated for homogeneity of variance between the non-filter and median filter processing of ASM images using the Fligner-Killeen test.

of images before filter processing in Fig. 1. The mean, SD, SNR, and CV obtained from the ROIs are listed in Table 4. The Fligner-Killeen test showed that the filter processing significantly reduced the variability in the ROIs ($p<0.01$, Table 4).

Similarity between ASM and DK images. The DK images after median filter processing scanned with 1.5 and 3.0T MRI are shown in Fig. 1. The image contrast of both DK images was visually and qualitatively similar to that of the ASM images shown in Fig. 1.

As the results of the quantitative evaluation of the similarity between ASM and DK images, Figure 2 provides a scatter plot of all of the ASM values in the ROI of the whole brain parenchyma of the ASM image on the vertical axis and all of the MK values in the ROI of the DK image on the horizontal axis. The Spearman's rank correlation coefficients between the ASM and MK values revealed the significantly weak correlations of 0.30 and 0.25 at 1.5 and 3.0T, respectively ($p<0.01$).

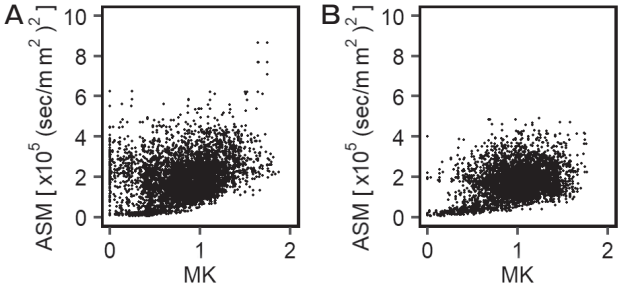

Fig. 2 Scatter plots of ASM and MK values. Each scatter plot created from images scanned with (**A**) 1.5T and (**B**) 3.0T MRI. ASM values were extracted from an ASM image created by protocol 3 with median filter processing. MK (mean kurtosis) values were extracted from a diffusion kurtosis image created with median filter processing.

Discussion

We developed the ASM as an MRI restricted diffusion-weighted imaging technique, similar to DK imaging. The present clinical study was conducted to evaluate the possibility of applying short-time imaging in clinical practice and to determine the capability of the ASM image creation software for clinical use, with the aim of applying the ASM in clinic settings. Our results identified the imaging sequences that can be used for short-time MR imaging. In addition, by using the ASM image creation software and post-processing filters, we were able to acquire ASM images of the human body that are similar to DK images.

The usefulness of DW images in clinical practice has been established mainly by the ADC map, which visualizes free diffusion [14-19]. The use of restricted diffusion-weighted images such as DK imaging, which visualizes the restricted diffusion of water molecules due to cell membranes and intracellular structures *in*

vivo, has been examined in clinical studies [3-7]. Yoshimura *et al.* developed the principle of ASM based on basic MRI studies of a bio-phantom, and they reported that the ASM may provide images of restricted diffusion that are as accurate as DK imaging [8]. Hamada *et al.* described the ASM image creation software based on Yoshimura's principle, and they succeeded in creating ASM images of a bio-phantom [10]. In the aforementioned studies, it was necessary to acquire images with sufficient spatial resolution and a high SNR because the bio-phantom was much smaller than the human body, and a sequence with an imaging time of > 30 min was used. In MRI examinations, it is essential to develop a new short imaging sequence to avoid the effects of body motion during imaging.

In the present study, we developed a short-time ASM imaging sequence for the human head to achieve the same imaging time as the head DW imaging used for ADC maps in clinical practice. Since the visual evaluation and the Spearman's rank correlation coefficient showed that the difference in protocols had little effect on the image quality, we selected protocol 3 with the shortest imaging time (the lowest number of b-values) as the short-time imaging sequence for ASM. As a result, the clinical ASM image of the head could be scanned in 3 min 10 sec at 1.5T MRI. Burdette *et al.* reported that there was little difference between images scanned with two b-values and those scanned with six b-values in terms of imaging the ADC map of the brain [20]. We speculate that the number of b-values did not affect the image quality in the ASM image created from the ADC map since the difference in the number of b-values did not affect the image quality of the ADC map. As we set the number of segments to 5 in order to reduce the susceptibility artifacts of 3.0T, the imaging time of 3.0T is twice as long as that of 1.5T. It might be effective to reduce the number of segments if it is necessary to further shorten the imaging time of 3.0T.

Diffusion images, including DK images, are affected by the noise in the original DW image [21-24]. Each diffusion image must be corrected for noise due to the bias caused by the noise. It has been reported that salt-and-pepper noise occurs in DK images [25], and that the use of median filter is effective for reducing this noise [26]. Diffusional Kurtosis Estimator (ver. 2.6.0; Center for Biomedical Imaging, Medical University of South Carolina, Charleston, SC, USA) [27], one of the software programs available for creating DK images, also applies median filter processing to DK images. We thus applied median filter processing to the ASM image in the present study, and its usefulness was evaluated. The median filter processing visually and qualitatively reduced the salt-and-pepper noise. In addition, the large variation in pixel values was significantly improved quantitatively.

We observed a weak correlation between the ASM and MK values in the heads of the two volunteers. The mean square displacement of water molecules in a three-dimensional space follows the Einstein-Smoluchowski Eq. (4) [28]:

$$<x^2> = 6 \times D \times t \quad (4)$$

where $<x^2>$ is the mean square displacement, D is the diffusion coefficient, and t is the diffusion time. The Stokes-Einstein equation [29] indicates that the diffusion coefficient of water at 37°C is 3×10^{-3} mm^2/sec. As the body temperature of our present subjects was ~37°C, the mean square displacement could be calculated from Eq. (4). The difference between the squared roots of the mean square displacement of the 'basic' and 'modify' sequences is 5.7 μm at 1.5T. The ASM image depicts this difference. On the other hand, DK imaging depicts deviation from the normal distribution as MK, which is calculated from the association between the b-value and the signal intensity [1,2]. ASM and DK imaging are thus based on different principles, which suggests that different levels of restricted diffusion may be depicted. Apoptotic bodies formed during apoptosis are less than a few micrometers in size, and the ASM and DK might be useful for the diagnosis and early determination of the effects of treatment for malignant lymphoma with apoptotic expression [30]. It is necessary to evaluate the usefulness of the ASM in clinical trials for diseases such as brain tumors, for which the clinical availability of DK imaging is well known. It is also necessary to consider the possibility of using the ASM as a new diagnostic method for diseases that are difficult to diagnose with conventional ADC maps and DK imaging. For this purpose, the widespread of ASM software and clinical research are indispensable.

This study has several limitations. The first is the limitation in ASM imaging in the setting used. There are numerous limitations in selecting different effective diffusion times for clinical MRI. In multiple clinical MR images, the effective diffusion time can be changed only within a limited range, mainly by changing the

b-value, and the degree of freedom is low. Other devices for experiments such as 7T allow the setting of large differences in the effective diffusion time [31]; however, these high-field devices have not been widely used in clinical practice. The second study limitation is that the ASM imaging was conducted on healthy subjects. DK and ASM imaging are useful for patients with diseases that exhibit restricted diffusion. In the present study, there were no pixels with strong restricted diffusion with MK values ~2. Clinical studies of patients are needed to validate the comparison of DK imaging with ASM imaging. A third study limitation is the use of median filter processing as a post-processing tool. Median filter processing reduces the noise qualitatively and quantitatively, but it changes the absolute values of multiple pixels in the ASM image as a computational value based on the principle behind the generation of ASM images. Clinical studies of patients are thus necessary to determine the effect of post-processing on the degree of disease depiction as a diagnosis. In addition, several types of post-processing filters have been proposed, and studies regarding the selection of the optimal post-processing filter for ASM imaging are also needed.

In conclusion, we investigated the DW imaging sequence for the human head in healthy subjects and developed a short-time imaging sequence that can be applied in future clinical studies of ASM imaging. To the best of our knowledge, this study is the first to report the application of ASM images for the human body. The short-time imaging sequence and the ASM image-generation software may be useful for future clinical studies of patients with different diseases.

Acknowledgments. We thank Dr. Kazuhide Yamamoto (Okayama Saiseikai General Hospital, Okayama, Japan) and Dr. Mitsumasa Kaji (Okayama Diagnostic Imaging Center, Okayama, Japan) for their cooperation in obtaining image data. The study was supported by Grants-in-Aid for Scientific Research (nos. C22591335, 15K09924 and 19K0809801) from the Ministry of Health, Labour and Welfare of Japan.

References

1. Jensen JH, Helpern JA, Ramani A, Lu H and Kaczynski K: Diffusional kurtosis imaging: the quantification of non-gaussian water diffusion by means of magnetic resonance imaging. Magn Reson Med (2005) 53: 1432–1440.
2. Jensen JH and Helpern JA: MRI quantification of non-Gaussian water diffusion by kurtosis analysis. NMR Biomed (2010) 23: 698–710.
3. Wu Y, Kim J, Chan ST, Zhou IY, Guo Y, Igarashi T, Zheng H, Guo G and Sun PZ: Comparison of image sensitivity between conventional tensor-based and fast diffusion kurtosis imaging protocols in a rodent model of acute ischemic stroke. NMR Biomed (2016) 29: 625–630.
4. Yoshida M, Hori M, Yokoyama K, Fukunaga I, Suzuki M, Kamagata K, Shimoji K, Nakanishi A, Hattori N, Masutani Y and Aoki S: Diffusional kurtosis imaging of normal-appearing white matter in multiple sclerosis: preliminary clinical experience. Jpn J Radiol (2013) 31: 50–55.
5. Van Cauter S, Veraart J, Sijbers J, Peeters RR, Himmelreich U, De Keyzer F, Van Gool SW, Van Calenbergh F, De Vleeschouwer S, Van Hecke W and Sunaert S: Gliomas: diffusion kurtosis MR imaging in grading. Radiology (2012) 263: 492–501.
6. Jiang R, Jiang J, Zhao L, Zhang J, Zhang S, Yao Y, Yang S, Shi J, Shen N, Su C, Zhang J and Zhu W: Diffusion kurtosis imaging can efficiently assess the glioma grade and cellular proliferation. Oncotarget (2015) 6: 42380–42393.
7. Bai Y, Lin Y, Tian J, Shi D, Cheng J, Haacke EM, Hong X, Ma B, Zhou J and Wang M: Grading of gliomas by using monoexponential, biexponential, and stretched exponential diffusion-weighted MR imaging and diffusion kurtosis MR imaging. Radiology (2016) 278: 496–504.
8. Yoshimura Y, Kuroda M, Sugianto I, Khasawneh A, Bamgbose BO, Hamada K, Barham M, Tekiki N, Kurozumi A, Matsushita T, Ohno S, Kanazawa S and Asaumi J: Development of a novel method for visualizing restricted diffusion using subtraction of apparent diffusion coefficient values. Mol Med Rep (2019) 20: 2963–2969.
9. Khasawneh A, Kuroda M, Yoshimura Y, Sugianto I, Bamgbose BO, Hamada K, Barham M, Tekiki N, Konishi K, Sugimoto K, Ishizaka H, Kurozumi A, Matsushita, T, Ohno S, Kanazawa S and Asaumi J: Development of a novel phantom using polyethylene glycol for the visualization of restricted diffusion in diffusion kurtosis imaging and apparent diffusion coefficient subtraction method. Biomed Rep (2020) 13: 52.
10. Hamada K, Kuroda M, Yoshimura Y, Khasawneh A, Barham M, Tekiki N, Sugianto I, Bamgbose BO, Konishi K, Sugimoto K, Ishizaka H, Kurozumi A, Matsushita T, Ohno S, Kanazawa S and Asaumi J: Evaluation of imaging process for a novel subtraction method using apparent diffusion coefficient values. Acta Med Okayama (2021) 75: 139–145.
11. Porter DA and Heidemann RM: High resolution diffusion-weighted imaging using readout-segmented echo-planar imaging, parallel imaging and a two-dimensional navigator-based reacquisition. Magn Reson Med (2009) 62: 468–475.
12. Schneider CA, Rasband WS and Eliceiri KW: NIH Image to ImageJ: 25 years of image analysis. Nat Methods (2012) 9: 671–675.
13. Fligner MA and Killeen TJ: Distribution-free two-sample tests for scale. J Am Stat Assoc (1976) 71: 210–213.
14. Lutsep HL, Albers GW, DeCrespigny A, Kamat GN, Marks MP and Moseley ME: Clinical utility of diffusion-weighted magnetic resonance imaging in the assessment of ischemic stroke. Ann Neurol (1997) 41: 574–580.
15. Driessen JP, van Kempen PMW, van der Heijden GJ, Philippens MEP, Pameijer FA, Stegeman I, Terhaard CHJ, Janssen LM and Grolman W: Diffusion-weighted imaging in head and neck squamous cell carcinomas: a systematic review. Head Neck (2015) 37: 440–448.
16. Suh CH, Yun SJ, Jin W, Lee SH, Park SY and Ryu CW: ADC as

a useful diagnostic tool for differentiating benign and malignant vertebral bone marrow lesions and compression fractures: a systematic review and meta-analysis. Eur Radiol (2018) 28: 2890–2902.
17. Woodhams R, Matsunaga K, Kan S, Hata H, Ozaki M, Iwabuchi K, Kuranami M, Watanabe M and Hayakawa K: ADC mapping of benign and malignant breast tumors. Magn Reson Med Sci (2005) 4: 35–42.
18. Gibbs P, Liney GP, Pickles MD, Zelhof B, Rodrigues G and Turnbull LW: Correlation of ADC and T2 measurements with cell density in prostate cancer at 3.0 Tesla. Invest Radiol (2009) 44: 572–576.
19. Levy A, Medjhoul A, Caramella C, Zareski E, Berges O, Chargari C, Boulet B, Bidault F, Dromain C and Balleyguier C: Interest of diffusion-weighted echo-planar MR imaging and apparent diffusion coefficient mapping in gynecological malignancies: a review. J Magn Reson Imaging (2011) 33: 1020–1027.
20. Burdette JH, Elster AD and Ricci PE: Calculation of apparent diffusion coefficients (ADCs) in brain using two-point and six-point methods. J Comput Assist Tomogr (1998) 22: 792–794.
21. Anderson AW: Theoretical analysis of the effects of noise on diffusion tensor imaging. Magn Reson Med (2001) 46: 1174–1188.
22. Barmpoutis A and Zhuo J: Diffusion kurtosis imaging: robust estimation from DW-MRI using homogeneous polynomials. In: 2011 IEEE International Symposium on Biomedical Imaging: From Nano to Macro (2011): pp262–265.
23. Li X, Yang J, Gao J, Luo X, Zhou Z, Hu Y, Wu EX and Wan M: A robust post-processing workflow for datasets with motion artifacts in diffusion kurtosis imaging. PLoS One (2014) 9: e94592.
24. Glenn GR, Tabesh A and Jensen JH: A simple noise correction scheme for diffusional kurtosis imaging. Magn Reson Imaging (2015) 33: 124–133.
25. Masutani Y and Aoki S: Fast and robust estimation of diffusional kurtosis imaging (DKI) parameters by general closed-form expressions and their extensions. Magn Reson Med Sci (2014) 13: 97–115.
26. Gonzalez RC and Woods RE: Image enhancement in the spatial domain; in Digital Image Processing. 2nd Ed, Prentice Hall, New Jersey (2002) pp123–124.
27. Tabesh A, Jensen JH, Ardekani BA and Helpern JA: Estimation of tensors and tensor-derived measures in diffusional kurtosis imaging. Magn Reson Med (2011) 65: 823–836.
28. Islam MA: Einstein–Smoluchowski diffusion equation: a discussion. Phys Scr (2004) 70: 120–125.
29. Einstein A: Investigations on the theory of the Brownian movement. Fürth R Ed, Dover Publications Inc., New York (1956) pp81.
30. Sasaki T, Kuroda M, Katashima K, Ashida M, Matsuzaki H, Asaumi J, Murakami J, Ohno S, Kato H and Kanazawa S: In vitro assessment of factors affecting the apparent diffusion coefficient of Ramos cells using bio-phantoms. Acta Med Okayama (2012) 66: 263–270.
31. Branzoli F, Techawiboonwong A, Kan H, Webb A and Ronen I: Functional diffusion-weighted magnetic resonance spectroscopy of the human primary visual cortex at 7T. Magn Reson Med (2013) 69: 303–309.